Report

Current Biology

Force Transmission between Three Tissues Controls Bipolar Planar Polarity Establishment and Morphogenesis

Graphical Abstract

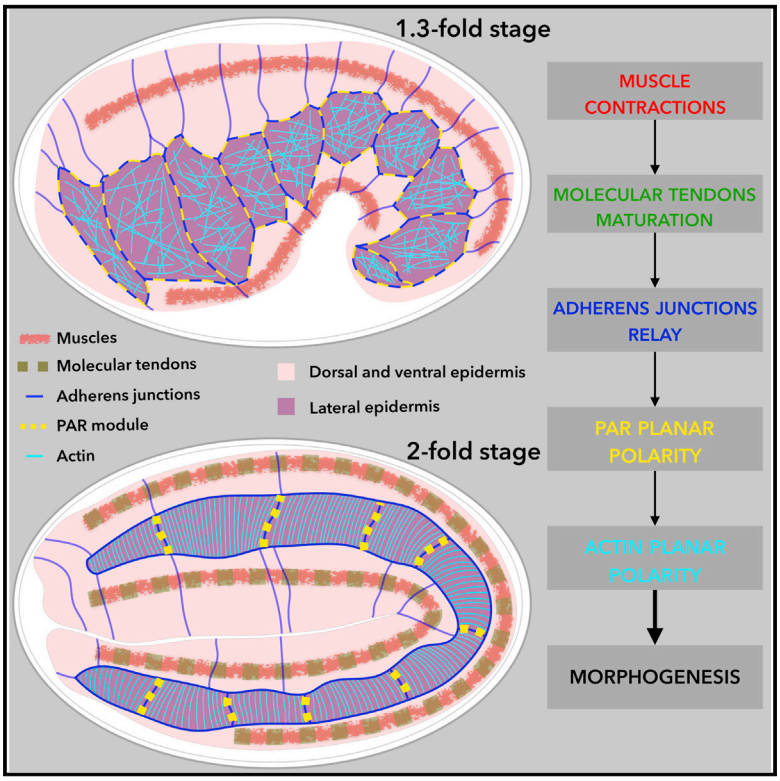

Highlights

- A mechanotransduction pathway coordinates the morphogenesis of three tissues
- The mechanical signal is initiated by muscle contractions
- It is transduced by molecular tendons and adherens junctions
- It controls bipolar planar polarity of PAR proteins and actin and, therefore, tension orientation

Authors

Ghislain Gillard, Ophélie Nicolle, Thibault Brugière, Sylvain Prigent, Mathieu Pinot, Grégoire Michaux

Correspondence

gmichaux@univ-rennes1.fr

In Brief

Gillard et al. describe a mechanotransduction signaling pathway initiated by muscle contractions that controls the establishment of bipolar planar polarity and coordinates the morphogenesis of three embryonic tissues during *C. elegans* embryogenesis.

Gillard et al., 2019, Current Biology *29*, 1360–1368
April 22, 2019 © 2019 Elsevier Ltd.
https://doi.org/10.1016/j.cub.2019.02.059

CellPress

CellPress

Current Biology
Report

Force Transmission between Three Tissues Controls Bipolar Planar Polarity Establishment and Morphogenesis

Ghislain Gillard,[1,3] Ophélie Nicolle,[1] Thibault Brugière,[1] Sylvain Prigent,[2] Mathieu Pinot,[1] and Grégoire Michaux[1,4,*]
[1]CNRS, Univ Rennes, IGDR (Institut de Génétique et Développement de Rennes) - UMR6290, 2 Avenue du Professeur Léon Bernard, 35000 Rennes, France
[2]Biogenouest, Bio-imaging axis, 16 Le Clos, 35590 Saint-Gilles, France, Univ Rennes, Microscopy Rennes Imaging Center, Biosit - UMS CNRS 3480/US INSERM 018, 2 Avenue du Professeur Léon Bernard, 35000 Rennes, France
[3]Present address: MRC LMB, Cambridge, UK
[4]Lead Contact
*Correspondence: gmichaux@univ-rennes1.fr
https://doi.org/10.1016/j.cub.2019.02.059

SUMMARY

How tissues from different developmental origins interact to achieve coordinated morphogenesis at the level of a whole organism is a fundamental question in developmental biology. While biochemical signaling pathways controlling morphogenesis have been extensively studied [1–3], morphogenesis of epithelial tissues can also be directed by mechanotransduction pathways physically linking two tissues [4–8]. *C. elegans* embryonic elongation requires the coordination of three tissues: muscles, the dorsal and ventral epidermis, and the lateral epidermis. Elongation starts by cell-shape changes driven by actomyosin contractions in the lateral epidermis [9, 10]. At mid-elongation, muscles become connected to the apical surface of the dorsal and ventral epidermis by molecular tendons formed by muscle integrins, extracellular matrix, and *C. elegans* hemidesmosomes (CeHDs). The mechanical signal generated by the onset of muscle contractions in the antero-posterior axis from mid-elongation is translated into a biochemical pathway controlling the maturation of CeHDs in the dorsal and ventral epidermis [11]. Consistently, mutations affecting muscle contractions or molecular tendons lead to a mid-elongation arrest [12]. Here, we found that the mechanical force generated by muscle contractions and relayed by molecular tendons is transmitted by adherens junctions to lateral epidermal cells, where it establishes a newly identified bipolar planar polarity of the apical PAR module. The planar polarized PAR module is then required for actin planar organization, thus contributing to the determination of the orientation of cell-shape changes and the elongation axis of the whole embryo. This mechanotransduction pathway is therefore essential to coordinate the morphogenesis of three embryonic tissues.

RESULTS AND DISCUSSION

At the beginning of the *C. elegans* embryonic elongation, the long axis of lateral epidermal cells is oriented along the dorso-ventral (D/V) axis. Actomyosin contractions in these cells progressively reduce cell length along the D/V axis and increase it along the antero-posterior (A/P) axis, inducing a 90° shift of the cell long axis from the D/V to the A/P axis. This process takes place in the plane of the apical membrane (Figures S1A and S1B). This orientation shift becomes obvious at the 2-fold stage and is concomitant with a progressive planar organization of actin fibers along the D/V axis in the lateral epidermis. While actin is partially disorganized at the 1.5-fold stage (Figures S1E–S1E'), it becomes mostly oriented along the D/V axis from the 2-fold stage (Figures S1F–S1G'), as was recently shown [13]. To identify the mechanisms underlying actin planar polarization, we looked for planar polarized factors in lateral epidermal cells. Previous studies have only identified a few, which are not required for embryonic elongation [14–16], while canonical planar cell polarity (PCP) is mostly required in neurons but not during elongation [17, 18]. During *Drosophila* embryonic morphogenesis, Bazooka/Par-3 becomes planar polarized in a bipolar manner [19]. Using CRISPR/Cas9 genome-edited strains to localize endogenous PAR-3::GFP, PAR-6::GFP and GFP::PKC-3 [20], we found that they exhibit bipolar planar polarity in lateral cells during elongation, accumulating on junctions between lateral cells (L-L junctions) but not on junctions between lateral and ventral or dorsal cells (L-D/V junctions) (Figures 1A–D, 1E, 1E', 1H, and 1H'); a similar localization was observed with a PAR-3::GFP line generated independently [21] (Figure S2H). We found that the PAR proteins progressively disappear from the L-D/V junctions between the 1.5- and the 2-fold stage (Figures 1A–1D and S2A–S2C''), while actin becomes oriented along the D/V axis (Figures S1E–S1G'). To test the role of apical PAR module components in their mutual planar localization, we showed that PAR-3 is essential for PAR-6 and PKC-3 recruitment at L-L junctions (Figures 1E–1J), while PAR-6 enables the recruitment of PAR-3 (Figures S2D–S2F).

Because we never observed PAR proteins' recruitment on the junctions between ventral or dorsal cells (Figures 1B, 1E, and 1H,

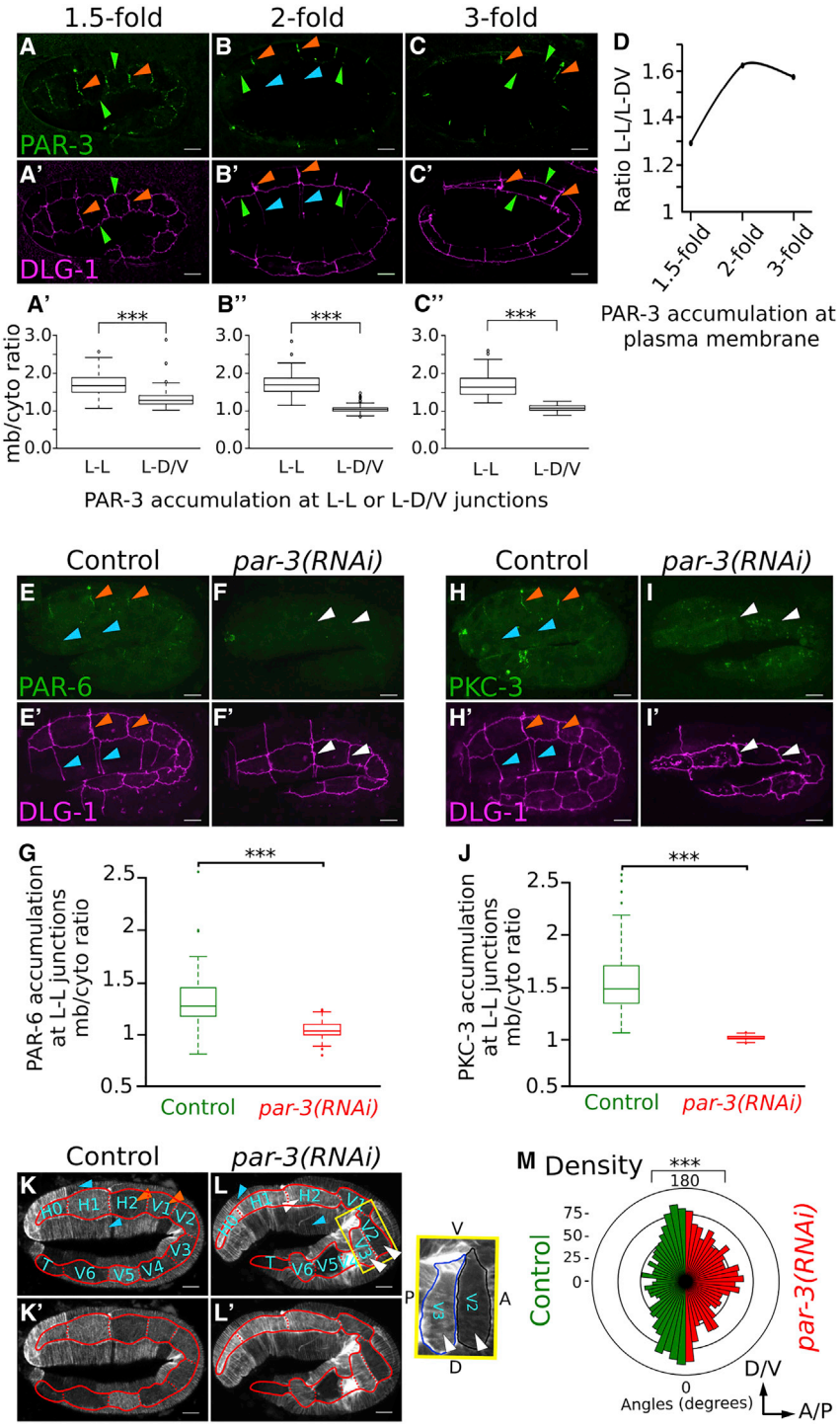

Figure 1. The PAR Module Is Planar Polarized in the Lateral Epidermis and Is Required for Actin Planar Polarity

(A–J) Observation of *C. elegans* embryos expressing endogenous PAR proteins in the epidermis at the level of the apical membrane during elongation. Orange arrowheads indicate L-L junctions; green arrowheads indicate the L-D/V junction; blue arrowheads indicate junctions between ventral cells; white arrowheads indicate the absence of PAR protein localization at L-L junctions.

(A–D) Endogenous PAR-3::GFP accumulates at L-L junctions (orange arrowheads) during elongation but is not visible at junctions between ventral cells (blue arrowheads); the signal on L-D/V junctions (green arrowheads) is weak at the 1.5-fold stage and decreases during elongation. DLG-1 (purple) is a junction marker. Quantifications (A"–C") were made by measuring the membrane/cytoplasm ratio ("mb/cyto ratio") between PAR-3 staining at L-L or L-D/V junction for each stage (n = 10 embryos 1.5-fold, 79 L-L and 137 L-D/V; n = 10 embryos 2-fold, 80 L-L and 113 L-D/V; n = 10 embryos 3-fold, 68 L-L and 113 L-D/V). The L-L / L-D/V ratio is shown in (D).

(E–J) PAR-3 is required for the recruitment of endogenous PAR-6::GFP (E–G) and GFP::PKC-3 (H–J) at L-L junctions. (G) and (J) correspond to quantifications of PAR-6 and PKC-3 recruitment, respectively, made by measuring the membrane/cytoplasm ratio ("mb/cyto ratio") at L-L junctions. (G) n = 22 control embryos, 66 L-L; n = 22 *par-3 (RNAi)* embryos, 66 L-L; (J) n = 30 control embryos, 90 L-L; n = 23 *par-3(RNAi)* embryos, 69 L-L.

(K–M) *par-3* depletion leads to actin misorientation (white arrowhead in L: n = 15 embryos, 67 cells, compared to orange arrowheads in control, K: n = 11 embryos, 34 cells) as confirmed by the associated quantification in (M). The yellow box shows two cells (V2 and V3) (white arrowheads) where actin is oriented in the A/P axis leading to a cell elongation in the D/V axis; this phenotype was observed in 9/21 embryos (0/23 in control embryos). Actin cables in ventral and dorsal cells (blue arrowheads) are not affected. Quantification of actin orientation; vertical axis, D/V orientation; horizontal axis, A/P orientation. See also Figures S1 and S2. All embryos are imaged at the 2-fold stage except in (A) and (C); anterior is to the left. Quantification results are shown as box plots; center line, median; box, first and third quartiles; whiskers, 10th and 90th percentiles; for actin orientation, plots show a percentage of counts in a given angle class/all counts, and there is one class for every 6° angle class. ***$p < 0.001$. Scale bars represent 5 μm.

blue arrows), we hypothesized that they have a specific function on L-L junctions in lateral cells. Genetic tools have already been used to analyze the role of PAR-3 and PAR-6 in epidermal cells during early elongation; however, the embryos arrested before the 2-fold stage [21, 22], precluding the analysis of their role in actin organization at later stages. We therefore depleted PAR-3 by RNAi using conditions leading to a 2-fold arrest (see STAR Methods). In these embryos, we observed that actin could be either disorganized or oriented in the A/P axis (Figures 1K–1M). Most strikingly, some cells were elongated in the D/V axis (Figure 1L) and systematically displayed A/P-oriented actin (19/19 D/V elongated cells; Figure S3M), strongly suggesting a correlation between orientation of actin filaments and the cell long axis. We concluded that the PAR module is planar polarized and that PAR-3 is required for actin planar reorganization in lateral epidermal cells.

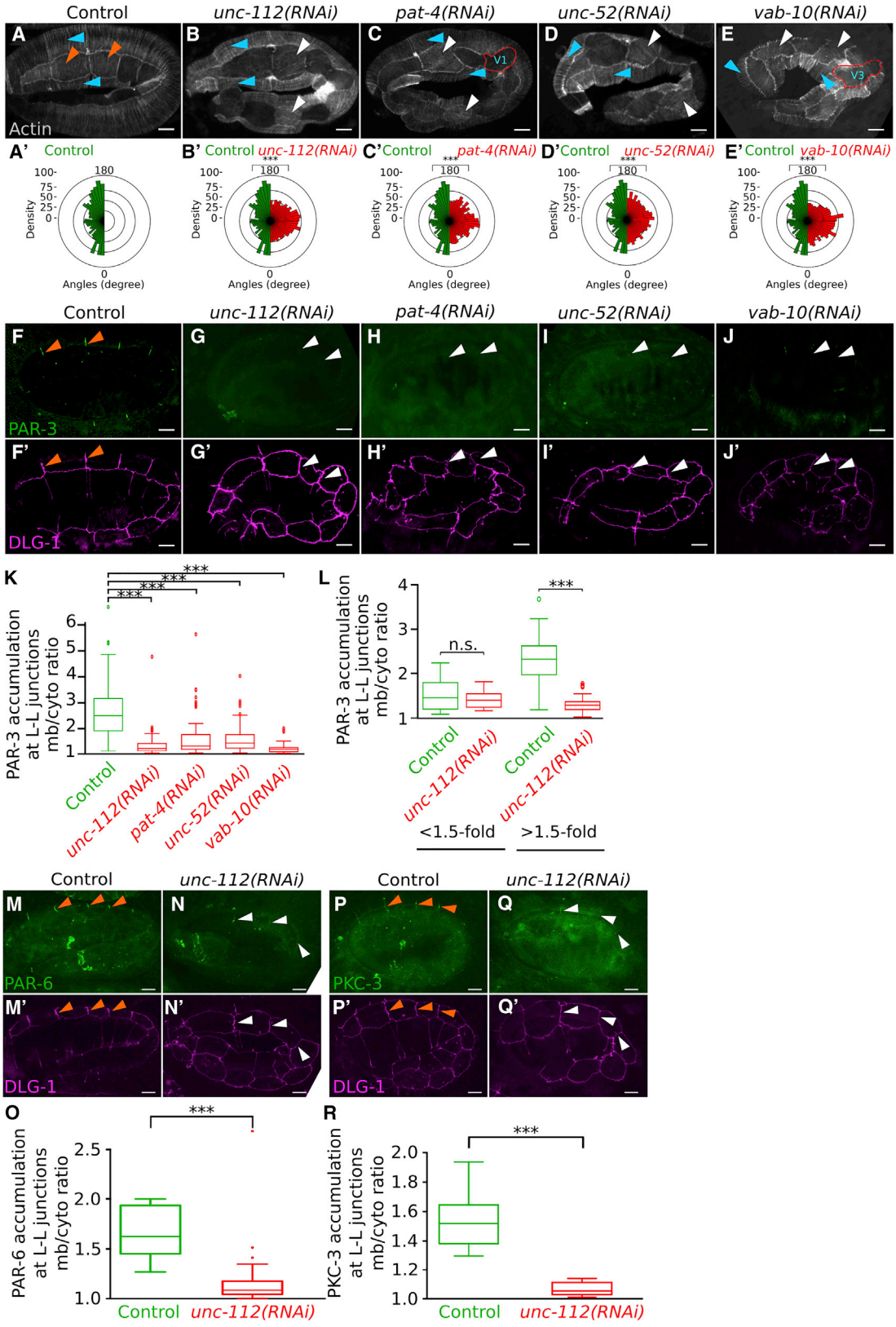

Figure 2. Muscles and Molecular Tendons Are Required for Lateral Epidermis Planar Polarity

(A–E) Actin organization in lateral epidermal cells at the 2-fold stage; actin is disorganized upon *unc-112* (B; n = 17 embryos, 61 cells), *pat-4* (C; n = 19 embryos, 72 cells), *unc-52* (D; n = 19 embryos, 61 cells), or *vab-10* (E; n = 17 embryos, 39 cells) depletion. Orange arrowheads indicate proper actin polarization in control

(legend continued on next page)

Despite the absence of a direct connection between muscles and the lateral epidermis (Figure S1C), there is a tight correlation in time between the onset of muscle contractions and the establishment of planar polarity from the 1.5-fold stage onward. Moreover, mutations affecting muscle contractions or components of molecular tendons trigger a 2-fold elongation arrest and were shown to induce an elongation of lateral cells in the D/V axis [23], as observed following PAR-3 depletion (Figure 1L). To examine the role of muscle contractions in actin organization, we first targeted genes expressed only in muscles (Figure S1D): *unc-112*/kindlin is essential for myosin heavy chain organization in myofilaments and PAT-3/β-integrin localization [24, 25], whereas the *pat-4*/ILK interacts with integrin adhesion complexes [26]. Depletion of these genes disrupted the elongation axis of some cells (Figure 2C, cell V1) and the planar polarity of actin in lateral epidermal cells (Figures 2A–2C'), suggesting that muscle contractions induce a mechanical signal transmitted to the lateral epidermis. We next investigated the function of CeHDs by depleting two genes expressed in the dorsal and ventral epidermis: *unc-52*, which encodes an extracellular matrix (ECM) perlecan secreted basolaterally [27], and *vab-10*, which is a spectraplakin homolog and a structural protein of CeHDs [28]. We found that these genes are also required for the elongation axis of some cells (Figure 2E, cell V3) and the planar polarity of actin in lateral epidermal cells (Figures 2D–2E'). We thus concluded that a biomechanical signal initiated by muscle contractions is relayed by molecular tendons in the dorsal and ventral epidermis and is required for actin organization in lateral epidermal cells.

We next addressed the functional relationship between muscle contractions and PAR proteins' planar localization. We found that *unc-112*, *pat-4*, *unc-52*, and *vab-10* are all required for the bipolar planar polarized localization of PAR-3 (Figures 2F–2K). To determine whether muscle contractions are required for the establishment or the maintenance of planar polarity, we quantified PAR-3 recruitment during elongation. In control embryos, PAR-3 is first localized in a junction-like manner at the apical side of lateral cells; planar polarity is then established from the 1.5-fold stage and peaks between the 2- and the 3-fold stage (Figure 1D). We abolished muscle contractions using an *unc-112(RNAi)* background and found that PAR-3 was weakly planar polarized both in control and *unc-112(RNAi)* embryos before the 1.5-fold stage, while *unc-112* becomes required to maintain PAR-3 localization on L-L junctions from the 1.5-fold stage (Figures 2L and S2G). This observation demonstrates that the biomechanical signal emitted by muscle contractions is not necessary for the initial PAR-3 plasma membrane recruitment but is required for the establishment of its robust bipolar planar polarity. Finally, we established that *unc-112* is also required for the planar polarity of PAR-6 and PKC-3 (Figures 2M–2R). We concluded that the planar polarized localization of the PAR module is controlled by a biomechanical signal initiated by muscle contractions and relayed by molecular tendons. The PAR module is then needed to properly orient actin in the D/V axis in the lateral epidermis. In line with the absence of the PAR module at the junctions between ventral or dorsal cells, orientation of actin cables in these cells does not require this pathway (Figure 1L and Figures 2A–2E, blue arrows).

In a subsequent RNAi screen designed to find new genes required for actin and PAR-3 planar polarity (Table S1), we identified the small GTPase RAB-1. RAB-1 depletion by RNAi induces a paralyzed 2-fold arrest (Figures S3A and S3B) and actin disorganization (Figures 3A–3C). We observed a frequent 90° shift in actin organization in the A/P axis (Figures 3B–3C); this phenotype was more frequent than it was in *par-3(RNAi)* embryos and is associated with cell axis elongation in the D/V rather than the A/P axis (Figures 3C and S3M). To evaluate the links between actin organization and cell elongation, we plotted lateral cell eccentricity and actin organization. We found that in control and *rab-1(RNAi)* embryos, there is a close correlation between actin organization in parallel filaments and robust cell eccentricity (Figure 3D), confirming a link between actin organization and cell elongation. We also found that *rab-1* depletion triggers a loss of PAR-3, PAR-6, and PKC-3 accumulation at L-L junctions (Figures 3E–3G and S3C–S3H). In yeast and mammalian cells, Rab1 regulates early secretion [29, 30], suggesting that it could be required for the secretion of molecular tendon components. We therefore examined the localization of the basolateral transmembrane receptor LET-805/myotactin and of the UNC-52/perlecan, both secreted by dorsal and ventral cells. We found that *rab-1* depletion leads to a disruption of UNC-52 and LET-805 localization (Figures 3H–3K). To confirm that the whole molecular tendon structure was affected, we showed that *rab-1* depletion also disrupts UNC-112 and PAT-3/β-integrin localization in muscles (Figures S3I–S3L). Our results therefore suggest that RAB-1 has a function in regulating CeHDs formation, presumably by controlling the secretion of at least some CeHD essential components; however, we cannot rule out a similar function in muscles in which it could also be required for PAT-3 secretion. The simultaneous loss of several molecular tendon components

cells (n = 11 embryos, 34 cells), while white arrowheads indicate cells in which actin is strongly disorganized; blue arrowheads indicate normal actin cable organization in ventral and dorsal cells; V1 and V3 indicate cells that are elongated in the D/V axis.

(A'–E') Quantification of actin orientation; vertical axis, D/V orientation; horizontal axis, A/P orientation.

(F–K) Depletion of *unc-112, pat-4, unc-52* or *vab-10* by RNAi leads to an absence of endogenous PAR-3::GFP at L-L junctions as depicted by white arrowheads compared to orange arrowheads in control. This absence of PAR-3 localization at the plasma membrane has been quantified in (K) (n = 20 control embryos, 112 L-L; n = 29 *unc-112(RNAi)* embryos, 188 L-L; n = 19 *pat-4(RNAi)* embryos, 132 L-L; n = 21 *unc-52(RNAi)* embryos, 106 L-L; n = 13 *vab-10(RNAi)* embryos, 82 L-L).

(L) Quantification of PAR-3::GFP accumulation at L-L junctions in control and *unc-112* depleted embryos at early stages (left, n = 21 control embryos, 25 *unc-112(RNAi)* embryos) and stages above the 1.5-fold stage (right, n = 29 control embryos, 29 embryos *unc-112(RNAi)*); 3 L-L junctions are quantified for each embryo; see also Figure S2G, which shows the same results as individual embryos with respect to the elongation index.

(M–R) The depletion of *unc-112* also affects the localization of endogenous PAR-6::GFP and GFP::PKC-3. In (O), n = 24 control embryos, 72 L-L; n = 21 *unc-112(RNAi)* embryos, 63 L-L. In (R), n = 25 control embryos, 75 L-L; n = 25 *unc-112(RNAi)* embryos, 75 L-L. See also Figure S2. All embryos were imaged and quantified at the 2-fold stage except in (L); anterior is to the left. Quantification results are shown as box plots; center line, median; box, first and third quartiles; whiskers, 10th and 90th percentiles; for actin orientation, plots show a percentage of counts in a given angle class/all counts, and there is one class for every 6° angle class. ***$p < 0.001$. Scale bars represent 5 μm.

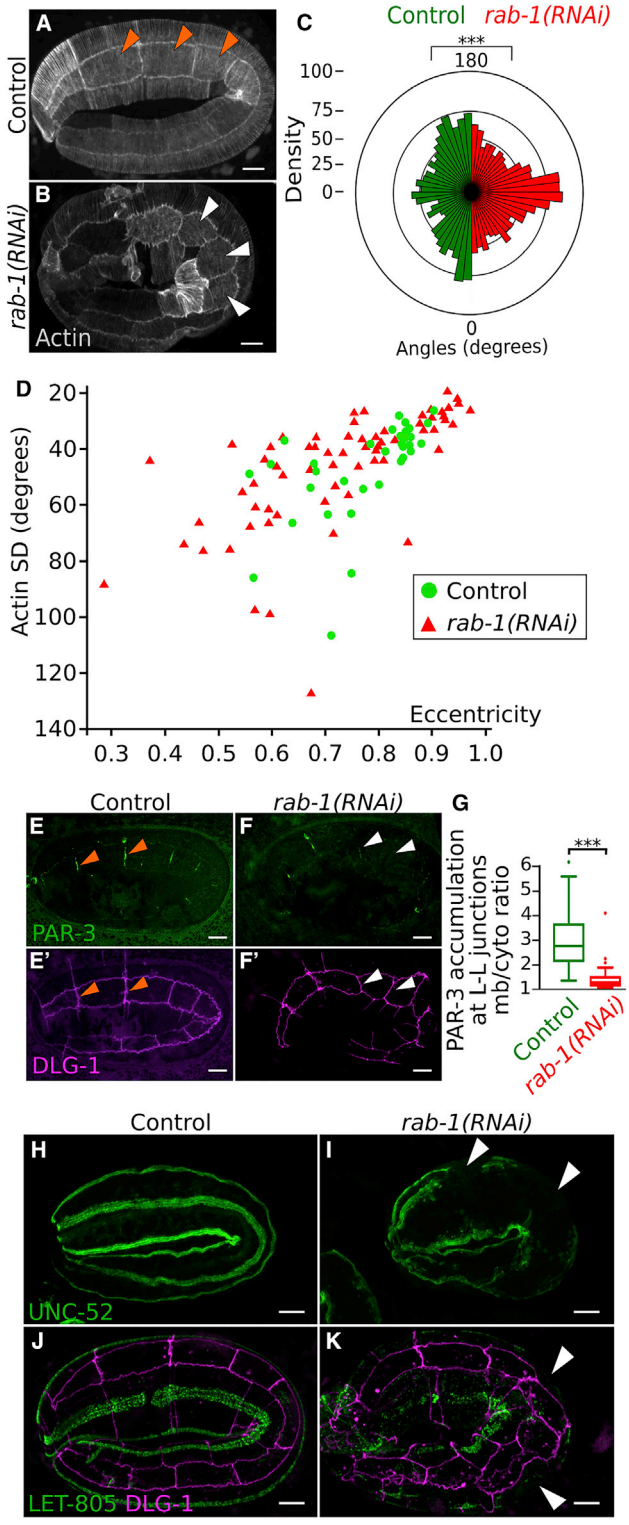

Figure 3. RAB-1 Is Required for Planar Polarity in the Lateral Epidermis through Molecular Tendon Component Localization

(A–C) *rab-1* depletion leads to actin disorganization in lateral epidermal cells at the 2-fold stage (n = 16 control embryos, 54 cells, orange arrowheads; n = 16 *rab-1(RNAi)* embryos, 69 cells, white arrowheads where actin is mostly oriented in the A/P axis). Note that a high proportion of cells display an A/P orientation of actin (C).

could explain the more severe actin phenotype observed in *rab-1(RNAi)* (Figure 3C) compared to the depletion of individual components (Figures 2A–2E), although we cannot exclude other functions for RAB-1 in the regulation of planar polarity.

We found that UNC-112, PAT-4, UNC-52, VAB-10, and RAB-1 control the onset and the transduction of the biomechanical signal generated by muscles leading to planar polarity establishment in lateral cells. However, the loss of PAR proteins and actin planar polarity could be explained by a global loss of epithelial polarity of lateral epidermal cells. We therefore examined junction integrity and apico-basal polarity using *unc-112(RNAi)* or *rab-1(RNAi)* to abolish muscle contractions or signal transduction, respectively. A combination of *in vivo* localization, fluorescence recovery after photo-bleaching (FRAP) experiments, and transmission electron microscopy (TEM) studies established that adherens junctions (AJs) were not affected (Figures 4A–4C and Figures S4A–S4M). We observed a slight decrease of E-cadherin membrane accumulation in *rab-1(RNAi)* (Figure 4D) but not *unc-112(RNAi)* embryos (Figure S4H), consistent with a role of RAB-1 in E-cadherin secretion. To further test the integrity of apico-basal polarity, we established that the apical transmembrane protein CHE-14 [31, 32] and the basolateral polarity determinant LET-413/Scribble [33] were also normally localized (Figures S4N–S4Q). Altogether, these results demonstrate that muscle biomechanical signaling is not required to establish or maintain junction integrity and apico-basal polarity in lateral epidermal cells.

We next sought to identify the possible signal transduction mechanism between the dorsal and ventral epidermis and the lateral epidermis. Given the biomechanical nature of the signal, we hypothesized that the putative transduction pathway could also be mechanical. For example, the apical extracellular matrix (aECM) might relay the deformations observed in dorsal and ventral cells upon muscle contractions [11]; however, depletion of aECM components triggers later elongation arrest and embryo bursting [34, 35], which are not consistent with our observations. AJs could also relay the biomechanical signal generated by muscles between the dorsal or ventral epidermis and the lateral epidermis. To test this possibility, we depleted HMP-1/α-catenin to induce a 2-fold stage arrest and block a putative

(D) Actin standard deviation and cell elongation (eccentricity) were plotted for control and *rab-1(RNAi)* embryos; each dot represents one cell (original data as in C); a Spearman test reveals a positive correlation ($p < 1.10^{-5}$) between the two parameters for both control and *rab-1(RNAi)* embryos.

(E–G) Endogenous PAR-3::GFP localization at L-L junctions observed in control embryos (orange arrowheads, n = 26 embryos, 78 junctions) is lost under *rab-1* depletion (white arrowheads, n = 12 embryos, 61 junctions). (G) corresponds to quantifications of PAR-3 accumulation at L-L junctions made by measuring the membrane/cytoplasm ratio ("mb/cyto ratio").

(H–K) *rab-1* depletion disrupts the localization of endogenous UNC-52 as revealed by immunostaining (H–I; n = 20 control embryos, n = 15 *rab-1(RNAi)* embryos) and of endogenous LET-805::GFP using a CRISPR line (J–K; n = 30 control embryos, n = 24 *rab-1(RNAi)* embryos). White arrowheads indicate areas of interrupted staining; DLG-1 is a junction marker. See also Figure S3 and Table S1. All embryos are imaged at the 2-fold stage; anterior is to the left. Quantification results are shown as box plots; center line, median; box, first and third quartiles; whiskers, 10th and 90th percentiles; for actin orientation, plots show a percentage of counts in a given angle class/all counts, and there is one class for every 6° angle class. ***$p < 0.001$. Scale bars represent 5 μm.

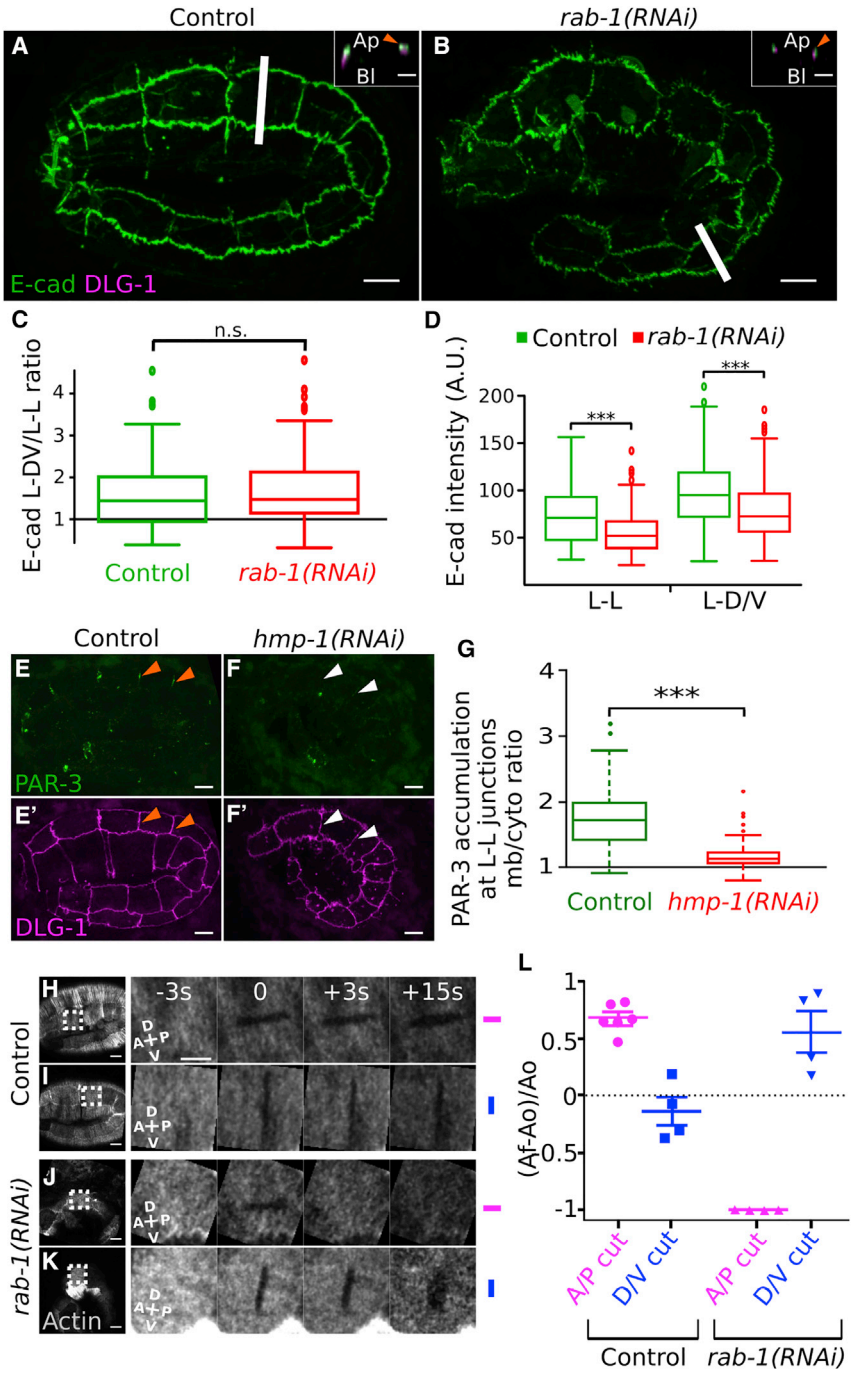

Figure 4. AJ Function in Signal Transduction and Role of Actin Planar Polarity in Tension Orientation

(A–D) E-cadherin (in green) remains apical upon *rab-1* depletion (B, n = 29 embryos) as in control embryos (A, n = 18). Small insets correspond to Z section represented by a white line in the associated picture: E-cadherin is localized above the junction marker DLG-1 (in purple). The quantification shows that the ratio of E-cadherin between L-D/V and L-L junctions remains intact under *rab-1* depletion (C). However, there is a slight decrease in E-cadherin overall accumulation at plasma membrane under *rab-1* depletion (D).

(E–G) Endogenous PAR-3::GFP localization at L-L junctions observed in control embryos (orange arrowheads, n = 26 embryos, 78 junctions) is lost upon *hmp-1* depletion (white arrowheads, n = 37 embryos, 111 junctions). DLG-1 is a junction marker. (G) corresponds to quantifications of PAR-3 recruitment made by measuring the membrane/cytoplasm ratio ("mb/cyto ratio") at L-L junctions.

(H–L) Laser nano-ablation experiments of the actin cytoskeleton in the lateral epidermis in control (H–I, actin oriented in the D/V axis) and *rab-1*-depleted (J–K, actin oriented in the A/P axis) embryos. Cuts were performed along the A/P axis (H, J in purple) or along the D/V axis (I, K in blue). These experiments have been quantified by measuring the relative expansion of the cut area over time; a value of 1 thus indicates an opening of the cut zone, while 0 indicates no opening, and −1 corresponds to closing (L; see STAR Methods for details). See also Figure S4. All embryos are imaged at the 2-fold stage; anterior is to the left. Quantification results are shown as box plots; center line, median; box, first and third quartiles; whiskers, 10th and 90th percentiles. ***$p < 0.001$. Scale bars represent 5 μm.

cell-cell signaling based on the E-cadherin/catenins complex. We found that PAR-3 failed to be recruited to L-L junctions in *hmp-1(RNAi)* 2-fold arrested embryos (Figures 4E–4G). We therefore propose the idea that the mechanical signal is transmitted to the lateral epidermis by AJs, although we cannot exclude the possibility that other mechanisms could also be implicated in this latter signal transduction step.

We finally assessed the consequences of actin disorganization on tension orientation in the lateral epidermis, which might explain the 90° shift observed in the elongation axis of some lateral cells. Using laser nano-ablation, we first showed that in control 2-fold stage embryos where actin is oriented in the D/V axis, a cut in the A/P axis leads to a systematic relaxation of the actin cytoskeleton, whereas a cut along the D/V axis does not lead to relaxation (Figures 4H–4I and 4L). These results reveal that tension forces are oriented along the D/V axis in the lateral epidermis at the 2-fold stage. We then exploited a phenotype frequently observed in *rab-1(RNAi)* embryos where actin is aligned along the A/P axis instead of the D/V axis. In *rab-1* depleted embryos displaying A/P-oriented actin, we observed a relaxation following a D/V cut suggesting a 90° shift of tension orientation (Figures 4K–4L). Surprisingly, the A/P cut led to a closure (Figures 4J and 4L), which could be explained by pushing forces exerted by the dorsal and ventral cells on the lateral epidermis; such a force would not be exerted by lateral cells, explaining why the reciprocal experiment in control embryos did not lead to a similar closure (Figures 4I and 4L). These results, together with the correlation between the cell elongation axis and actin organization (Figure 3D), strongly

support the hypothesis that actin orientation is the primary cause of the cell elongation axis, which is itself the main cause of the embryonic elongation axis. We therefore propose that the disorganization of actin in lateral cells observed upon disruption of the mechanical signal initiated by muscle contractions induces the arrest at the 2-fold stage.

We found that muscle contractions initiate a mechanical signal transmitted to the lateral epidermis through dorsal and ventral molecular tendons and AJs; this signal is essential to promote a planar organization of the PAR module and actin, thus regulating tension orientation in lateral cells. We have therefore identified a trans-tissular mechanotransduction signaling pathway required to coordinate morphogenesis between three tissues: muscles, the dorsal and ventral epidermis, and the lateral epidermis during *C. elegans* embryonic morphogenesis (Figure S4R). Interestingly, the mechanical signal generated by muscles is therefore at the origin of at least two different outcomes: maturation of CeHDs [11] and establishment of planar polarity in lateral cells. This pathway is very different from the canonical Wnt/PCP, Fat/Dachsous, and Toll receptor pathways that enable cells to establish vectorial/unipolar planar polarity [36, 37]. However, many other proteins have been found to be planar polarized in a bipolar manner, e.g., E-cadherin [38], myosin [19], and PAR-3 [19, 39] in *Drosophila*, or tropomodulin [14], microtubules, and NOCA-1 [15, 16] and the apical PAR module (this study) in *C. elegans*. Interestingly, there is a parallel between the mutual exclusion of PAR-3 and myosin in *Drosophila* [19, 40] and the apical PAR module and actin in *C. elegans* (this study), even if myosin is not polarized in lateral cells [13]. While in *Drosophila*, Rho kinase is required for PAR-3 planar polarity [41], the mechanism leading to the PAR module planar polarization is not yet identified in *C. elegans*. For instance, the often-PAR-associated CDC-42 GTPase has been proposed to play a role during early elongation, but its function was not investigated during later elongation [42]. Future work investigating the pathway(s) leading to the PAR module bipolar planar polarity downstream of AJs, and how PAR proteins could control actin organization in lateral cells, will be necessary to fully characterize this new mechanotransduction pathway.

Tissue mechanics and force transmission have been previously shown to be involved in *Drosophila* wing morphogenesis, where the wing-hinge retraction enables planar rearrangement from a radial to a proximal-distal-oriented polarity in the wing blade [5]; similarly, a mechanical input has been implicated in setting up planar polarity during *Drosophila* germ-band extension [4, 8, 41]. In a different context, a recent study demonstrated that a physical pressure exerted by proliferating dermal cells controls the patterning of the avian skin [43]. However, in all these examples, the tissue-wide tension is generated in direct connection with the target tissue. Our results show a more complex signal-transduction pathway wherein the tension generated by muscles is relayed along two tissues, first in the inside-to-outside orientation through molecular tendons and then in the D/V axis through AJs. Interestingly, smooth muscles lie below or inside many tissues, such as the skin, the intestine, the respiratory organs, or the reproductive tracts, where they could be essential for planar polarity establishment in surrounding epithelial tissues throughout the animal kingdom. We therefore believe that this new signaling pathway implicated in force transmission through several tissues could be conserved in other organisms.

STAR★METHODS

Detailed methods are provided in the online version of this paper and include the following:

- KEY RESOURCES TABLE
- CONTACT FOR REAGENT AND RESOURCE SHARING
- EXPERIMENTAL MODEL AND SUBJECT DETAILS
- METHOD DETAILS
  - Overview
  - Plasmid construction and strains
  - RNAi
  - Immunostaining
  - Electron microscopy
  - Confocal microscopy
  - FRAP experiments
  - Laser nano-ablations
- QUANTIFICATION AND STATISTICAL ANALYSIS
  - Overview
  - Fluorescence intensity measurements
  - Actin orientation in lateral epidermal cells
  - FRAP quantifications
  - Actin organisation and cell elongation axis
  - Laser nano-ablation quantifications
  - Statistical analysis

SUPPLEMENTAL INFORMATION

Supplemental Information can be found with this article online at https://doi.org/10.1016/j.cub.2019.02.059.

ACKNOWLEDGMENTS

We thank Yohanns Bellaïche, Jean-Louis Bessereau, Aurélien Bidaud-Meynard, Juan Manuel Gomez, Michel Labouesse, Roland Le Borgne, Anne Pacquelet, and Sophie Quintin for helpful discussions and critical reading of the manuscript; we also thank Yann Le Cunff for his help in statistical analysis. We are grateful to Liam Coyne, Anushae Syed, Ken Kemphues, and Michel Labouesse for sharing unpublished CRISPR/Cas9 genome edited GFP fusion strains; Jeff Hardin, Renaud Legouis, and Jeremy Nance for strains; and Sara Bouizakarne for her help in analyzing actin orientation/cell eccentricity. We thank Maïté Carre-Pierrat and the UMS3421 (Lyon) for generating the *Cbr-rab-1* expressing strain. Some strains were provided by the CGC, which is funded by NIH Office of Research Infrastructure Programs (P40 OD010440; University of Minnesota, US). We thank the photon and electron microscopy facilities of the Microscopy Rennes Imaging Center (MRIC). This work was supported by the Ligue contre le Cancer Grand Ouest 22/29/35/41/72, the Fondation ARC (PJA 20161204670) and the Fondation Maladies Rares; we also receive institutional funding from the Centre National de la Recherche Scientifique (CNRS) and the Université de Rennes 1. G.G. was funded by the Ministère de l'Enseignement Supérieur et de la Recherche (2012–2015) and the Ligue Nationale Contre le Cancer (2015–2016).

AUTHOR CONTRIBUTIONS

G.G. and G.M. designed the experiments. G.G., O.N., T.B., and G.M. performed experiments and data analysis. S.P. and M.P. helped to perform quantifications and design laser nano-ablation experiments. G.G. and G.M. wrote the manuscript. G.M. supervised the study.

DECLARATION OF INTERESTS

The authors declare no competing interests.

Received: September 25, 2018
Revised: January 22, 2019
Accepted: February 27, 2019
Published: March 28, 2019

REFERENCES

1. Hubaud, A., and Pourquié, O. (2014). Signalling dynamics in vertebrate segmentation. Nat. Rev. Mol. Cell Biol. *15*, 709–721.
2. Petit, F., Sears, K.E., and Ahituv, N. (2017). Limb development: a paradigm of gene regulation. Nat. Rev. Genet. *18*, 245–258.
3. Schmid, T., and Hajnal, A. (2015). Signal transduction during C. elegans vulval development: a NeverEnding story. Curr. Opin. Genet. Dev. *32*, 1–9.
4. Collinet, C., Rauzi, M., Lenne, P.F., and Lecuit, T. (2015). Local and tissue-scale forces drive oriented junction growth during tissue extension. Nat. Cell Biol. *17*, 1247–1258.
5. Aigouy, B., Farhadifar, R., Staple, D.B., Sagner, A., Röper, J.C., Jülicher, F., and Eaton, S. (2010). Cell flow reorients the axis of planar polarity in the wing epithelium of Drosophila. Cell *142*, 773–786.
6. Olguín, P., Glavic, A., and Mlodzik, M. (2011). Intertissue mechanical stress affects Frizzled-mediated planar cell polarity in the Drosophila notum epidermis. Curr. Biol. *21*, 236–242.
7. Sagner, A., Merkel, M., Aigouy, B., Gaebel, J., Brankatschk, M., Jülicher, F., and Eaton, S. (2012). Establishment of global patterns of planar polarity during growth of the Drosophila wing epithelium. Curr. Biol. *22*, 1296–1301.
8. Butler, L.C., Blanchard, G.B., Kabla, A.J., Lawrence, N.J., Welchman, D.P., Mahadevan, L., Adams, R.J., and Sanson, B. (2009). Cell shape changes indicate a role for extrinsic tensile forces in Drosophila germband extension. Nat. Cell Biol. *11*, 859–864.
9. Diogon, M., Wissler, F., Quintin, S., Nagamatsu, Y., Sookhareea, S., Landmann, F., Hutter, H., Vitale, N., and Labouesse, M. (2007). The RhoGAP RGA-2 and LET-502/ROCK achieve a balance of actomyosin-dependent forces in C. elegans epidermis to control morphogenesis. Development *134*, 2469–2479.
10. Piekny, A.J., Johnson, J.L., Cham, G.D., and Mains, P.E. (2003). The Caenorhabditis elegans nonmuscle myosin genes nmy-1 and nmy-2 function as redundant components of the let-502/Rho-binding kinase and mel-11/myosin phosphatase pathway during embryonic morphogenesis. Development *130*, 5695–5704.
11. Zhang, H., Landmann, F., Zahreddine, H., Rodriguez, D., Koch, M., and Labouesse, M. (2011). A tension-induced mechanotransduction pathway promotes epithelial morphogenesis. Nature *471*, 99–103.
12. Vuong-Brender, T.T., Yang, X., and Labouesse, M. (2016). C. elegans embryonic morphogenesis. Curr. Top. Dev. Biol. *116*, 597–616.
13. Vuong-Brender, T.T., Ben Amar, M., Pontabry, J., and Labouesse, M. (2017). The interplay of stiffness and force anisotropies drives embryo elongation. eLife *6*, e23866.
14. Cox-Paulson, E.A., Walck-Shannon, E., Lynch, A.M., Yamashiro, S., Zaidel-Bar, R., Eno, C.C., Ono, S., and Hardin, J. (2012). Tropomodulin protects α-catenin-dependent junctional-actin networks under stress during epithelial morphogenesis. Curr. Biol. *22*, 1500–1505.
15. Quintin, S., Wang, S., Pontabry, J., Bender, A., Robin, F., Hyenne, V., Landmann, F., Gally, C., Oegema, K., and Labouesse, M. (2016). Non-centrosomal epidermal microtubules act in parallel to LET-502/ROCK to promote C. elegans elongation. Development *143*, 160–173.
16. Wang, S., Wu, D., Quintin, S., Green, R.A., Cheerambathur, D.K., Ochoa, S.D., Desai, A., and Oegema, K. (2015). NOCA-1 functions with γ-tubulin and in parallel to Patronin to assemble non-centrosomal microtubule arrays in C. elegans. eLife *4*, e08649.
17. Chen, C.H., He, C.W., Liao, C.P., and Pan, C.L. (2017). A Wnt-planar polarity pathway instructs neurite branching by restricting F-actin assembly through endosomal signaling. PLoS Genet. *13*, e1006720.
18. Shah, P.K., Tanner, M.R., Kovacevic, I., Rankin, A., Marshall, T.E., Noblett, N., Tran, N.N., Roenspies, T., Hung, J., Chen, Z., et al. (2017). PCP and SAX-3/robo pathways cooperate to regulate convergent extension-based nerve cord assembly in C. elegans. Dev. Cell *41*, 195–203.e3.
19. Zallen, J.A., and Wieschaus, E. (2004). Patterned gene expression directs bipolar planar polarity in Drosophila. Dev. Cell *6*, 343–355.
20. Rodriguez, J., Peglion, F., Martin, J., Hubatsch, L., Reich, J., Hirani, N., Gubieda, A.G., Roffey, J., Fernandes, A.R., St Johnston, D., et al. (2017). aPKC cycles between functionally distinct PAR protein assemblies to drive cell polarity. Dev. Cell *42*, 400–415.e9.
21. Achilleos, A., Wehman, A.M., and Nance, J. (2010). PAR-3 mediates the initial clustering and apical localization of junction and polarity proteins during C. elegans intestinal epithelial cell polarization. Development *137*, 1833–1842.
22. Totong, R., Achilleos, A., and Nance, J. (2007). PAR-6 is required for junction formation but not apicobasal polarization in C. elegans embryonic epithelial cells. Development *134*, 1259–1268.
23. Hresko, M.C., Williams, B.D., and Waterston, R.H. (1994). Assembly of body wall muscle and muscle cell attachment structures in Caenorhabditis elegans. J. Cell Biol. *124*, 491–506.
24. Rogalski, T.M., Mullen, G.P., Gilbert, M.M., Williams, B.D., and Moerman, D.G. (2000). The UNC-112 gene in Caenorhabditis elegans encodes a novel component of cell-matrix adhesion structures required for integrin localization in the muscle cell membrane. J. Cell Biol. *150*, 253–264.
25. Williams, B.D., and Waterston, R.H. (1994). Genes critical for muscle development and function in Caenorhabditis elegans identified through lethal mutations. J. Cell Biol. *124*, 475–490.
26. Mackinnon, A.C., Qadota, H., Norman, K.R., Moerman, D.G., and Williams, B.D. (2002). C. elegans PAT-4/ILK functions as an adaptor protein within integrin adhesion complexes. Curr. Biol. *12*, 787–797.
27. Rogalski, T.M., Williams, B.D., Mullen, G.P., and Moerman, D.G. (1993). Products of the unc-52 gene in Caenorhabditis elegans are homologous to the core protein of the mammalian basement membrane heparan sulfate proteoglycan. Genes Dev. *7*, 1471–1484.
28. Bosher, J.M., Hahn, B.S., Legouis, R., Sookhareea, S., Weimer, R.M., Gansmuller, A., Chisholm, A.D., Rose, A.M., Bessereau, J.L., and Labouesse, M. (2003). The Caenorhabditis elegans vab-10 spectraplakin isoforms protect the epidermis against internal and external forces. J. Cell Biol. *161*, 757–768.
29. Plutner, H., Cox, A.D., Pind, S., Khosravi-Far, R., Bourne, J.R., Schwaninger, R., Der, C.J., and Balch, W.E. (1991). Rab1b regulates vesicular transport between the endoplasmic reticulum and successive Golgi compartments. J. Cell Biol. *115*, 31–43.
30. Segev, N., Mulholland, J., and Botstein, D. (1988). The yeast GTP-binding YPT1 protein and a mammalian counterpart are associated with the secretion machinery. Cell *52*, 915–924.
31. Gillard, G., Shafaq-Zadah, M., Nicolle, O., Damaj, R., Pécréaux, J., and Michaux, G. (2015). Control of E-cadherin apical localisation and morphogenesis by a SOAP-1/AP-1/clathrin pathway in C. elegans epidermal cells. Development *142*, 1684–1694.
32. Michaux, G., Gansmuller, A., Hindelang, C., and Labouesse, M. (2000). CHE-14, a protein with a sterol-sensing domain, is required for apical sorting in C. elegans ectodermal epithelial cells. Curr. Biol. *10*, 1098–1107.
33. Legouis, R., Gansmuller, A., Sookhareea, S., Bosher, J.M., Baillie, D.L., and Labouesse, M. (2000). LET-413 is a basolateral protein required for the assembly of adherens junctions in Caenorhabditis elegans. Nat. Cell Biol. *2*, 415–422.
34. Mancuso, V.P., Parry, J.M., Storer, L., Poggioli, C., Nguyen, K.C., Hall, D.H., and Sundaram, M.V. (2012). Extracellular leucine-rich repeat proteins are required to organize the apical extracellular matrix and maintain epithelial junction integrity in C. elegans. Development *139*, 979–990.

35. Vuong-Brender, T.T.K., Suman, S.K., and Labouesse, M. (2017). The apical ECM preserves embryonic integrity and distributes mechanical stress during morphogenesis. Development *144*, 4336–4349.

36. Aw, W.Y., and Devenport, D. (2017). Planar cell polarity: global inputs establishing cellular asymmetry. Curr. Opin. Cell Biol. *44*, 110–116.

37. Butler, M.T., and Wallingford, J.B. (2017). Planar cell polarity in development and disease. Nat. Rev. Mol. Cell Biol. *18*, 375–388.

38. Levayer, R., Pelissier-Monier, A., and Lecuit, T. (2011). Spatial regulation of Dia and Myosin-II by RhoGEF2 controls initiation of E-cadherin endocytosis during epithelial morphogenesis. Nat. Cell Biol. *13*, 529–540.

39. Besson, C., Bernard, F., Corson, F., Rouault, H., Reynaud, E., Keder, A., Mazouni, K., and Schweisguth, F. (2015). Planar cell polarity breaks the symmetry of PAR protein distribution prior to mitosis in Drosophila sensory organ precursor cells. Curr. Biol. *25*, 1104–1110.

40. Fernandez-Gonzalez, R., Simoes, Sde.M., Röper, J.C., Eaton, S., and Zallen, J.A. (2009). Myosin II dynamics are regulated by tension in intercalating cells. Dev. Cell *17*, 736–743.

41. Simões, Sde.M., Blankenship, J.T., Weitz, O., Farrell, D.L., Tamada, M., Fernandez-Gonzalez, R., and Zallen, J.A. (2010). Rho-kinase directs Bazooka/Par-3 planar polarity during Drosophila axis elongation. Dev. Cell *19*, 377–388.

42. Zilberman, Y., Abrams, J., Anderson, D.C., and Nance, J. (2017). Cdc42 regulates junctional actin but not cell polarization in the *Caenorhabditis elegans* epidermis. J. Cell Biol. *216*, 3729–3744.

43. Shyer, A.E., Rodrigues, A.R., Schroeder, G.G., Kassianidou, E., Kumar, S., and Harland, R.M. (2017). Emergent cellular self-organization and mechanosensation initiate follicle pattern in the avian skin. Science *357*, 811–815.

44. Bouvrais, H., Chesneau, L., Pastezeur, S., Fairbrass, D., Delattre, M., and Pécréaux, J. (2018). Microtubule feedback and LET-99-dependent control of pulling forces ensure robust spindle position. Biophys. J. *115*, 2189–2205.

45. Gomez, J.M., Chumakova, L., Bulgakova, N.A., and Brown, N.H. (2016). Microtubule organization is determined by the shape of epithelial cells. Nat. Commun. *7*, 13172.

46. Brenner, S. (1974). The genetics of Caenorhabditis elegans. Genetics *77*, 71–94.

47. Fire, A., Xu, S., Montgomery, M.K., Kostas, S.A., Driver, S.E., and Mello, C.C. (1998). Potent and specific genetic interference by double-stranded RNA in Caenorhabditis elegans. Nature *391*, 806–811.

48. Kamath, R.S., and Ahringer, J. (2003). Genome-wide RNAi screening in Caenorhabditis elegans. Methods *30*, 313–321.

49. Shafaq-Zadah, M., Brocard, L., Solari, F., and Michaux, G. (2012). AP-1 is required for the maintenance of apico-basal polarity in the C. elegans intestine. Development *139*, 2061–2070.

50. Leung, B., Hermann, G.J., and Priess, J.R. (1999). Organogenesis of the Caenorhabditis elegans intestine. Dev. Biol. *216*, 114–134.

51. Cetera, M., Ramirez-San Juan, G.R., Oakes, P.W., Lewellyn, L., Fairchild, M.J., Tanentzapf, G., Gardel, M.L., and Horne-Badovinac, S. (2014). Epithelial rotation promotes the global alignment of contractile actin bundles during Drosophila egg chamber elongation. Nat. Commun. *5*, 5511.

STAR★METHODS

KEY RESOURCES TABLE

REAGENT or RESOURCE	SOURCE	IDENTIFIER
Antibodies		
MH2 Mouse anti-perlecan UNC-52	DSHB	RRID:AB_528432
Alexa 488 goat anti-Mouse IgG	ThermoFisher	Cat# A11001; RRID:AB_2534069
Bacterial and Virus Strains		
E. coli: OP50	Caenorhabditis Genetics Center	RRID:WB-STRAIN:OP50
Library Efficiency® DH5α™ Competent Cells	Invitrogen	Cat# 18263012
Library Efficiency® DB3.1™ Competent Cells	Invitrogen	Cat# 11782-018
Chemicals, Peptides, and Recombinant Proteins		
Bovine Serum Albumin (BSA) Protease Free Lyophilised	BioWest	Cat# P6155
Polybead® Microspheres 0.10 μm	Polysciences	Cat# 00876-15
Critical Commercial Assays		
Gateway® BP Clonase® Enzyme Mix	ThermoFisher	Cat# 11789020
Phusion® High-Fidelity PCR Master Mix with GC Buffer	New England Biolabs	Cat# M0532L
Experimental Models: Organisms/Strains		
C. briggsae: Strain ANA020	[44]	ANA020
C. elegans: Strain wild-type N2	Caenorhabditis Genetics Center	RRID:WB-STRAIN:N2_(ancestral)
C. elegans: Strain DM5115	Caenorhabditis Genetics Center	RRID:WB-STRAIN:DM5115
C. elegans: Strain FL16: *[che-14::gfp + rol-6(su1006)]; unc-119(ed3)III; mcIs46[dlg-1::rfp ; unc-119(+)]*	This study	FL16
C. elegans: Strain FL36: *jcIs11[vab-9::gfp + rol-6(su1006)]; unc-119(ed3) III; mcIs46[dlg-1::rfp, unc119(+)]*	This study	FL36
C. elegans: Strain FL301: *mcIs97[hmr-1::gfp]; unc-119(ed3) III; mcIs46[dlg-1::rfp, unc119(+)]*	This study	FL301
C. elegans: Strain FL309: *rab-1(ok3750) V/nT1[qIs51](IV;V); mcIs97[hmr1::gfp]; unc-119(ed3) III; mcIs46[dlg-1::rfp, unc119(+)]*	This study	FL309
C. elegans: Strain FL311: *mcIs50 [lin-26p::vab-10(actin-binding domain)::GFP + myo-2p::GFP + pBluescript]; unc-119(ed3) III; mcIs46[dlg-1::rfp; unc-119(+)]*	This study	FL311
C. elegans: Strain FL350: *par-3(it298[par-3::gfp]) III; unc-119(ed3) III; mcIs46[dlg-1::rfp; unc-119(+)]*	This study	FL350
C. elegans: Strain FL351: *par-6(it310[par-6::gfp])I; unc-119(ed3) III; mcIs46[dlg-1::rfp; unc-119(+)]*	This study	FL351
C. elegans: Strain FL352: *pkc-3(it309[gfp::pkc-3]II; nc-119(ed3) III; mcIs46[dlg-1::rfp; unc-119(+)]*	This study	FL352
C. elegans: Strain FL367: *let-805(mc73)III; unc-119(ed3) III; mcIs46[dlg-1::rfp; unc-119(+)]*	This study	FL367
C. elegans: Strain ML623: *let-413::gfp + rol-6(su1006)*	[34]	ML623
C. elegans: Strain NK358	Caenorhabditis Genetics Center	RRID:WB-STRAIN:NK358
C. elegans: Strain VC3070	Caenorhabditis Genetics Center	RRID:WB-STRAIN:VC3070
Oligonucleotides		
Cbr-rab-1 for cloning in pDONR 221 Fw: 5′-GGGGACAAGTTTG TACAAAAAAGCAGGCTCATATTTTTTGACCCACTTTGAGGG-3′	This study	N/A
Cbr-rab-1 for cloning in pDONR 221 Rev: 5′-GGGGACCACTTTG TACAAGAAAGCTGGGTCAGGCAACATGTGGTTCTACATCCC-3′	This study	N/A
rab-1(ok3750) PCR Fw: 5′-AGGGGAGAGAAAAGACAGCA-3′	This study	N/A
rab-1(ok3750) PCR Rev: 5′-CTCCTGTTGCTGACCGATTT-3′	This study	N/A
Recombinant DNA		
Plasmid: *Cbr-rab-1* (in pDONR221)	This study	N/A

(*Continued on next page*)

Continued

REAGENT or RESOURCE	SOURCE	IDENTIFIER
Software and Algorithms		
Excel (https://www.microsoft.com/en-gb/)	Microsoft	RRID:SCR_016137
Fiji 1.0 (http://fiji.sc/)	NIH Image	RRID:SCR_002285
ImageJ 1.4 (https://imagej.net/Welcome)	NIH Image	RRID:SCR_003070
Inkscape 0.48 (http://inkscape.org/)	Inkscape	RRID:SCR_014479
MATLAB (https://www.mathworks.com/products/matlab.html)	MathWorks	RRID:SCR_001622
MATLAB script for actin organization and cell elongation axis	Gomez et al. [45]	RRID:SCR_001622
R Project for Statistical Computing (https://www.r-project.org/)	R Core Team, 2016	RRID:SCR_001905
ggplot2: Various R Programming Tools for Plotting Data (https://cran.r-project.org/web/packages/ggplot2/index.html)	R Package	RRID:SCR_014601

CONTACT FOR REAGENT AND RESOURCE SHARING

Further information and requests for resources and reagents should be directed to and will be fulfilled by the Lead Contact, Grégoire Michaux (gmichaux@univ-rennes1.fr).

EXPERIMENTAL MODEL AND SUBJECT DETAILS

C. elegans and *C. briggsae* strains were used in this study. All analyzed animals were hermaphrodites and at the embryonic stage at the time of observations. Figure legends indicate the precise embryonic stage for each experiment.

Health/immune status: not applicable
Subjects were never involved in previous procedures
All embryos were drug and test naive
The genotypes of the strains used in this study are detailed in the Key Resource Table.
Species/strain of experimental models: all embryos were derived from the *C. elegans* N2 Bristol isolate. The *C. briggsae* strain is derived from AF16 Indian isolate.
Husbandry conditions: *C. elegans* and *C. briggsae* strains were maintained and crossed on NGM plates seeded with *E. coli* OP50 at 20°C [46].

METHOD DETAILS

Overview

All experiments were replicated at least three times except for the *par-6* depletion which was replicated two times. No strategy was used for randomization or stratification; no blinding was used, and sample-size were not estimated. No data were excluded during quantifications.

Plasmid construction and strains

The *C. briggsae* version of *rab-1* (called *Cbr-rab-1*) was amplified from the ANA020 strain [44] by PCR with the Phusion Master Mix then cloned in the Gateway pDONR p221 with the Gateway BP Clonase Enzyme Mix. The construct was injected at 5 ng/μL together with the *rol-6(su1006)* marker at 100 ng/μL in the *C. elegans* N2 strain.

RNAi

Embryonic RNAi was performed by feeding using the Ahringer-Source BioScience library [47–49]; RNAi was induced in young adults and the phenotypes observed in the next generation (F1). L4440 corresponds to the standard control RNAi feeding strain. For some genes (e.g., *par-3, par-6*) the duration of the RNAi treatment was adapted (< 24 h) to observe elongation phenotypes while avoiding earlier developmental phenotypes usually associated with these genes; *rab-1(RNAi)* was induced for about 20 h to avoid the sterility triggered in the parental generation. All embryos observed and used for quantifications were 7-10 h old, corresponding to 1.5- to 3-fold embryos in a WT strain; as a control we checked that there was not expression of the *myo-2p::GFP* transgene which is expressed from the 3-fold stage and present in the FL311 strain used to localize ABD::GFP. RNAi efficiency was checked by observing the induction of a developmental arrest whenever such a phenotype was expected based on previous reports. To test the specificity of the *rab-1(RNAi)* we scored the embryonic lethality observed following *Cel-rab-1(RNAi)* in an N2 strain and in a strain expressing *Cbr-rab-1* as presented in Figures S3A–S3B.

Immunostaining

Fixation of embryos was performed using the freeze-crack methanol protocol [50]. Briefly, embryos were squeezed for 2 min before being frozen in liquid nitrogen, fixed in methanol for 20 min and washed in PBS. After a blocking step in PBS-Tween 0.2% supplemented with 1% BSA for 20 min, embryos were incubated with the primary antibody at 4°C overnight then with the secondary antibody at 1 h at 37°C in a wet chamber. Embryos were finally mounted in 10 μL Mowiol. We used the anti-UNC-52 MH2 (1/50) monoclonal antibody from DSHB (University of Iowa, USA). Alexa Fluor 488 antibody (ThermoFisher) was used as secondary antibody. All antibodies were diluted in PBS-Tween 0.2%.

Electron microscopy

To prepare samples for electron microscopy experiments embryos were fixed by high pressure freezing followed by freeze substitution, flat embedding to allow antero-posterior orientation and sectioning [49]. Control (n = 3) and *rab-1(RNAi)* (n = 4) embryos were observed. Each embryo was sectioned every 5-7 μm to ensure that different cells were observed in different 5-7 μm segments; 3 segments were examined for each embryo. The pictures in Figures S4L–S4M are representative of all the sections observed. Observations were performed on a Jeol JEM1400 equipped with a Gatan Orius SC1000 camera.

Confocal microscopy

Confocal observations were performed on 1.5-, 2-, and 3-fold stage embryos. From the 1.5-fold stage embryos start moving due to muscle contractions; from the 1.8-fold stage they move too rapidly for imaging and these movements completely prevent obtaining movies of the progressive planar polarization of the PAR module and of actin. To image these embryos, we added bacteria to the mounting medium M9. This treatment results in progressive hypoxia leading to muscle inactivity and immobilisation. Embryos were then imaged using Leica (Wetzlar, Germany) SPE, SP5 or SP8 confocals equipped with 63X/1.4 HCX PL APO objectives (LAS AF software). The SP5 and SP8 confocals are equipped with hybrid detectors which were used to image the low signals generated by the genome-edited strains expressing PAR-3::GFP, PAR-6::GFP and GFP::PKC-3 at the endogenous level. They were also used to image ABD::GFP at the highest possible resolution with a low background. All images were examined using ImageJ 1.43 or Fiji 1.0 and assembled using the Inkscape software. No image manipulation was performed except adjusting contrast and brightness in an homogeneous way throughout the picture.

FRAP experiments

FRAP experiments were performed on 1.5-fold stage embryos just before the onset of muscle contractions. We used an inverted Nikon Ti-E microscope equipped with a Spinning-disk CSU-X1 and a single-point scanning head to allow laser microirradiation. Embryos were imaged with a 63X/1.4 PLAN APO objective and fluorescence was collected with an sCMOS ORCA Flash 4.0 camera. The FRAP was performed on a whole junction with 100% laser power, 50 iterations and a line thickness of 2, in the iLAS software in Metamorph. Post-FRAP images were acquired every 10 s.

Laser nano-ablations

Laser nano-ablation experiments were performed on 2-fold stage embryos. Because at that stage embryos move too rapidly for imaging we prevented movements by adding bacteria to the mounting medium M9. This treatment results in progressive hypoxia leading to muscle inactivity and immobilization. To perform ablations, we selected embryos which had just stopped moving and used an inverted Leica SP5 microscope equipped with a Pulsed laser Mai Tai HP Ti. Embryos were imaged with a 63X/1.4 HCX PL APO objective. Laser nano-ablations were performed at 800 nm with a single iteration. Images were acquired every 1.27 s.

QUANTIFICATION AND STATISTICAL ANALYSIS

Overview

The percentage of embryos displaying a phenotype was obtained either by direct observation or after quantification. All quantifications were performed on images acquired in independent experiments (no embryo was measured repeatedly). Gaussian distribution and similar variances were tested before performing statistical analysis.

Fluorescence intensity measurements

Quantifications were performed using ImageJ 1.43 or Fiji 1.0 along lines (length 5-10 μm, width 0.3 μm) over the membrane and cytoplasmic parts of at least three cells for each embryo. The membrane quantification was normalized to the cytoplasmic background; a ratio of 1 therefore indicates no specific membrane localization. In Figure 4D and Figure S4H we measured intensity along the membranes and plotted these numbers directly, without normalization to the cytoplasm.

Actin orientation in lateral epidermal cells

Actin orientation was measured in MATLAB using custom-routines [51]. Briefly local directors representing actin alignment were determined as follows for each cell: a cell was properly oriented and broken in small overlapping windows of 2.6*2.6 μm and the 2D FFT of each filtered window was calculated, giving a range of angles whose values are given compared to the dorso-ventral axis. Each count is the dominant angle for a particular 2.6 μm square analysis window, and each count is plotted. Representative

cell with actin local directors are shown in Figure S1. The data are shown on plots as a percentage of counts in a given angle class / all counts and there is one class for every 6° angle (30 classes to cover 180°) for all the plots.

FRAP quantifications

Quantifications were made manually in ImageJ by measuring the mean intensity of the bleached junction after background subtraction.

Actin organisation and cell elongation axis

We exploited a MATLAB script written by Gomez et al. [45]. We used it to recognize and analyze the cytoskeleton organization in 8-bit images of embryonic lateral cells. Inputs files are two subfolders that contain an image of a cell border, an image of the embryo and the other contains the cytoskeleton projection inside a given cell. The script recognizes the cytoskeleton and the cell borders using the generated mask. The script fits the cell as an ellipse and calculate the eccentricity and the standard deviation SD. SD measures actin alignment with respect to the major axis of the ellipse. The eccentricity calculated using MATLAB is defined as the ratio of the distance between the foci of the ellipse and its major axis length. If the eccentricity is 0, the ellipse is a circle and if it is equal to 1 the ellipse is equivalent to a segment. To do so, the signal of each pixel is extracted using the cell mask and the gradient of the signal is calculated using a Sobel filter (5x5). The magnitude M depends on the signal gradient along x and y and is used to quantify the direction of its pixel and its changes. We plotted the eccentricity of each cell (elongation axis) as a function of the standard deviation of the actin signal in the same cell in order to obtain the correlation between the cell elongation axis and actin orientation

Laser nano-ablation quantifications

For quantifications, the cut zone was manually tracked over time in ImageJ and the relative expansion was calculated as follows: $(I_{15} - I_0)/I_0$ where I is the small axis of the cut zone; 0 and 15 correspond to the first picture after the cut and the picture after 15 s, respectively. A value of 1 thus indicates an opening due to relaxation, while 0 indicates no relaxation and -1 corresponds to a closing by contraction and/or compression; compression could be passive, possibly due to pushing forces exerted by the dorsal and ventral epidermis and contraction could be due to actin dynamics within lateral cells.

Statistical analysis

To determine whether the data met assumptions of the statistical approaches used we first analyzed the data distribution and the variances. Parametric t tests were used when samples had a Gaussian distribution and similar variances. Other cases were treated using non-parametric Wilcoxon tests. Actin distribution was treated using a X^2 test. A Spearman correlation test was used to determine the correlation between actin standard deviation and cell eccentricity. Significance is indicated as follows: $^*p < 0.05$, $^{**}p < 0.01$, $^{***}p < 0.001$. Quantification results are shown as boxplots: center line: median; box: first and third quartiles; whiskers: 10th and 90th percentiles. In all Figure legends, n refers to the number of different embryos analyzed for a particular experiment. These legends also clearly indicate the number of junctions/cells analyzed for each experiment.